Fast matter-antimatter separation via Weibel-induced plasma filamentation

Oliver Mathiak , ^{1,*} Lars Reichwein , ^{2,1} and Alexander Pukhov ¹ Institut für Theoretische Physik I, Heinrich-Heine-Universität Düsseldorf, 40225 Düsseldorf, Germany ² Peter Grünberg Institut (PGI-6), Forschungszentrum Jülich, 52425 Jülich, Germany

(Received 10 February 2025; revised 5 May 2025; accepted 2 July 2025; published 20 August 2025)

We study the separation of matter and antimatter driven by the growth of the Weibel instability in a matter-antimatter plasma. The plasma under consideration comprises protons and antiprotons initially at rest, along with a relativistic stream of leptons (electrons and positrons). This stream is maintained by an external force, potentially originating from phenomena such as a photon wind. Our findings reveal the rapid onset of a Weibel-type instability, leading to a distinct separation of matter and antimatter. Results from our particle-in-cell simulations are compared with an analytical model based on the linearized magnetohydrodynamics equations.

DOI: 10.1103/wsly-16yn

I. INTRODUCTION

The imbalance between matter and antimatter in the observable Universe remains one of the most profound unanswered questions in modern physics. It is well established that the observable Universe is predominantly composed of matter, with antimatter appearing only in trace amounts [1–3]. This asymmetry is puzzling, as standard mechanisms of matterantimatter creation, such as pair production, do not inherently favor one over the other.

One hypothesis suggests that the Universe may contain regions dominated by either matter or antimatter, which could have formed in the early Universe when matter-antimatter plasmas were prevalent [4]. Furthermore, magnetic fields, which are ubiquitous throughout the Universe [5–7], are believed to have originated during this primordial matter-antimatter plasma era [8,9].

Matter-antimatter plasmas also play a central role in some of the most energetic astrophysical phenomena, such as gamma-ray bursts (GRBs). These bursts are thought to arise from ultrarelativistic winds of matter-antimatter plasma ejected by extreme cosmic objects such as black holes, pulsars, and quasars [10,11]. GRBs are extraordinarily luminous, allowing their detection over vast distances—billions of light years—providing rare insights into the early Universe [12].

Despite their significance, studying such phenomena through telescopes is inherently challenging due to their transient and distant nature. This has spurred growing interest in creating matter-antimatter plasmas in laboratory settings, enabling the study of high-energy astrophysical processes such as collisionless shocks, magnetic reconnection, and plasma

instabilities [13–18]. Advances in high-intensity laser technology have made laboratory astrophysics increasingly feasible and relevant [19]. Moreover, plasma instabilities have been shown to be of importance for particle acceleration in laser-plasma interactions [20].

Although significant progress has been made in generating electron-positron pairs in the laboratory [13,21], creating a full-fledged matter-antimatter plasma remains a substantial challenge. Plasma behavior requires the plasma size to exceed the Debye length, necessitating a sufficiently large number of pairs. Theoretical investigations, e.g., by Kendl *et al.*, have shown that the dynamics in electron-positron plasmas in (inhomogeneous) magnetic fields can be very complex [22].

In this study, inspired by the conditions of the early Universe, we investigate a matter-antimatter plasma composed of electrons, positrons, protons, and antiprotons. The protons and antiprotons are initially stationary, while the leptons stream collinearly in one direction, driven by high-energy photons exerting a constant, charge-independent force via Compton scattering.

Using two- and three-dimensional particle-in-cell (PIC) simulations, we demonstrate the filamentation of the plasma due to counterpropagating currents and the exponential growth of density instabilities, specifically a Weibel instability. Additionally, we observe the emergence of a distinct high-energy peak in the lepton energy spectrum, driven by the stopping field.

Finally, we support our numerical findings with an analytical model describing the initial growth of the instability, derived from the linearization of magnetohydrodynamic (MHD) equations.

II. SETUP

We consider a matter-antimatter plasma, consisting of protons and antiprotons that are initially at rest and relativistic electrons and positrons that stream colinearly in the *z* direction. The plasma is initially homogeneous and charge neutral. Consequently, the plasma is initially in equilibrium. However,

Published by the American Physical Society under the terms of the Creative Commons Attribution 4.0 International license. Further distribution of this work must maintain attribution to the author(s) and the published article's title, journal citation, and DOI.

^{*}Contact author: oliver.mathiak@hhu.de

this equilibrium is highly unstable due to the counterpropagating currents of the leptons. In a homogeneous plasma, the currents from the electrons and positrons cancel each other exactly. However, small perturbations of the density will lead to effective currents and a strong repelling force and a perturbation in the charge density. To regain equilibrium, the repelled leptons will pull the oppositely charged hadrons with them, which leads to a separation of matter and antimatter.

In this paper, we neglect other effects such as matterantimatter annihilation: For an ultrarelativistic lepton with energy $\varepsilon \gg m_e c^2$ the cross section of the annihilation process [23] is

$$\sigma_{\rm ann} = \frac{\alpha^2 \pi \hbar^2}{m_e \varepsilon} \left[\ln \frac{2\varepsilon}{m_e c^2} - 1 \right] + O\left(\frac{\ln 2\varepsilon / m_e c^2}{\varepsilon / m_e c^2} \right). \tag{1}$$

Accordingly, the characteristic time of electron-positron annihilation is

$$\tau_{\rm ann} = \frac{1}{c\sigma n_0} = \frac{m_e \varepsilon}{\alpha^2 \pi c \hbar^2 n_0} \left(\ln \frac{2\varepsilon}{m_e c^2} - 1 \right)^{-1} \,. \tag{2}$$

Annihilation effects become negligible when the characteristic time of the plasma $\tau_p = \omega_p^{-1} = \sqrt{\frac{m_e}{4\pi n_0 e^2}}$ is much smaller than that of the annihilation process. Because the plasma period and annihilation time depend on the density in a different order, we obtain an upper limit for the plasma density, where this assumption is valid,

$$n_0 \ll \frac{4m_e \varepsilon^2}{\alpha^2 \pi c \hbar^3} \left(\ln \frac{2\varepsilon}{m_e c^2} - 1 \right)^2.$$
 (3)

For a particle energy of $\varepsilon=100~\text{MeV}\approx 200 m_e c^2$ this results in an upper density limit of $n_{\text{max}}\sim 10^{40}~\text{cm}^{-3}$.

An analogous estimation can be made for the much heavier hadrons, where the calculation of the annihilation cross section is much more complicated. However, from the literature [24–28] we can estimate the cross section for protonantiproton annihilation to be $\sigma_{p^+p^-} \sim 0.5$ b. Using this and the plasma frequency for hadrons gives an upper bound for the hadron density $n_{\rm max} \sim 10^{37} \ {\rm cm}^{-3}$.

In our setup, we assume that the leptons got accelerated by a flux of streaming photons via Compton scattering. Furthermore, we assume a flux of photons to persist during the simulation that interact with the leptons by exerting a constant, charge independent force.

Let us consider a single Compton scattering event of a photon, moving in the z direction with energy $\varepsilon = E_\gamma/m_ec^2$ resulting in a scattering angle θ . The change in momentum of the lepton in the z direction is then

$$\frac{\Delta p_z}{m_e c} = \varepsilon - \frac{\varepsilon \cos \theta}{1 + \varepsilon (1 - \cos \theta)},\tag{4}$$

while the transversal momentum change will average out over many scattering events.

The effective force resulting from the scattering of photons is

$$f_{\rm CS} = \frac{dp_z}{dt} = n_{\gamma}c \int d\Omega \Delta p_z \frac{d\sigma}{d\Omega},\tag{5}$$

with the photon density n_{γ} and the angular differential cross section $d\sigma/d\Omega$.

The cross section of the Compton scattering processes is given by

$$\frac{d\sigma}{d\Omega} = \frac{1}{2} r_0^2 \frac{\varepsilon'^2}{\varepsilon^2} \left(\frac{\varepsilon'}{\varepsilon} + \frac{\varepsilon}{\varepsilon'} - \sin^2 \theta \right), \tag{6}$$

with ε' being the energy of the lepton after the scattering event and $r_0 = e^2/m_ec^2 \approx 2.82 \times 10^{-15}$ m the classical electron radius. For a photon energy of $\varepsilon = m_ec^2$ and a photon density of $n_\gamma = 10^{30}$ cm⁻³ this will result in a force $f_{\rm CS} \sim 10^{-6}$ N.

III. PARTICLE-IN-CELL SIMULATIONS

We conduct particle-in-cell (PIC) simulations using the code VLPL [29,30] in order to study the behavior of the proposed matter-antimatter mixture. In the subsequent sections, we first investigate the filamentation dynamics. Later on, examine the peak formation in the tail of the lepton energy spectra.

We simulate the plasma on a square domain with length $2\pi \cdot 100k_p^{-1}$, where $k_p = \omega_p/c$ and time step $t = 0.005\omega_p^{-1}$ for up to $\sim 12\,000\omega_p^{-1}$. The grid step is chosen as $h_x = h_y = 1.5k_p^{-1}$, with 64 particles per cell for leptons and 32 particles for hadrons, resulting in a total of $\sim 3 \times 10^7$ numerical particles.

The leptons have an initial longitudinal momentum of $p_{\parallel} = 100 m_e c$, parallel to the z axis and the force.

Thus, our transverse grid steps do resolve the relativistic plasma skin length $l_s \approx \sqrt{\gamma} k_p^{-1} = 10 k_p$. The transverse momenta of the leptons follow a normal distribution with mean zero and $\sigma = p_{\perp}/m_e c = 1, 0.1, 0.01$ for different simulation runs. A constant force $f = 0.1 m_e c \omega_p$, that acts in the z direction, is applied to the leptons.

All properties scale uniformly with the simulation's normalization length k_p^{-1} , which defines the density and force. The force has been chosen such that it is small compared to the driving forces of the separation, but large enough to stabilize the separation mechanism by counteracting the stopping force on the leptons. Therefore, in our analytic approach we can neglect the force, but the leptons retain their longitudinal momentum for longer, leading to a more pronounced separation of matter and antimatter. Due to the isotropic and stationary nature of the problem we use a Yee-lattice-based Maxwell solver [31] and quadratic momentum pusher. Additionally, to simulate an infinite plasma, we set periodic boundary conditions throughout, both for particles and fields.

Figure 1 shows the electron density at different stages of the simulation. At the early stage $(\omega_p t \leqslant 60)$, the density perturbation $\delta n = n - n_0$ is noiselike with $\delta n \ll n_0$. In the intermediate stage $(\omega_p t \leqslant 300)$, δn grows larger than n_0 due to the agglomeration of matter and antimatter in small, distinct patches. In the later stages of the simulation, those patches merge into larger, contiguous filaments that are separated by bands of strong electromagnetic fields (see Fig. 2). The leptons pull the hadrons along with them, such that filaments that are larger than the plasma skin depth are on average charge neutral. As a result, the hadron density is almost identical to the corresponding lepton density.

In three dimensions, a similar filamentation occurs with an added structure in the z direction. Figure 3 schematically

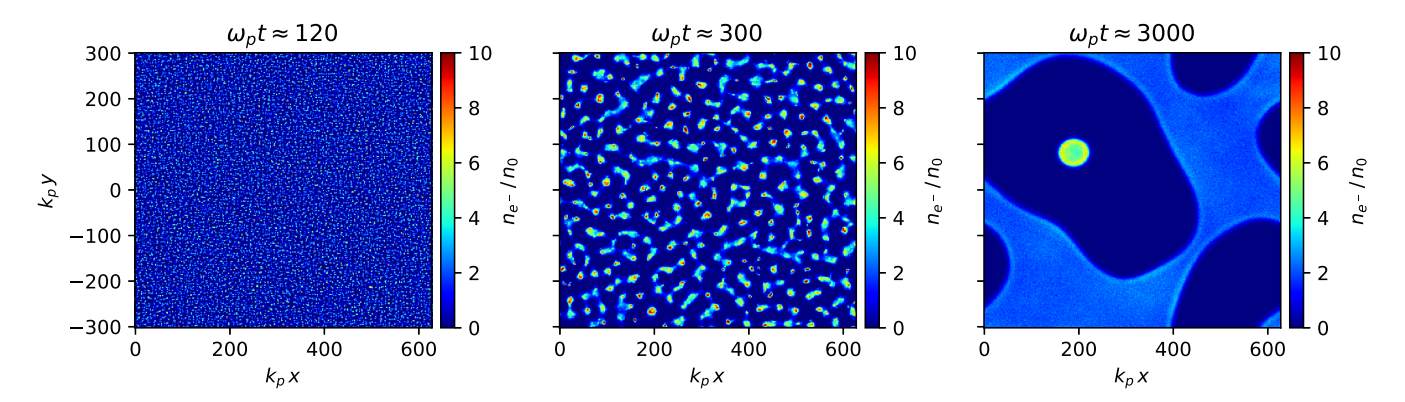


FIG. 1. Evolution of the electron density for a two-dimensional (2D) simulation. The color bars are clipped for easier comparison of the various stages.

shows the electron density in three dimensions after $\omega_p t \sim 3000$. An identical filamentation in the x-y plane, perpendicular to the direction of momentum, occurs with an added, yet less dominant, filamentation in the z direction. This implies that the two-dimensional case is sufficient to understand the underlying mechanics. Therefore, and for computational efficiency, we will restrict ourselves to 2D simulations.

During the early stage ($\omega_p t \leq 100$), the difference in density is still small and can be treated as a perturbation. This is essentially a Weibel instability [32].

It is therefore expected that at the beginning, the instability grows exponentially. This is confirmed for $\omega_p t \leq 100$ considering Fig. 4. We run the simulation for different initial transverse momenta both in two and three dimensions. While a higher p_{\perp} initially leads to a faster separation of matter and antimatter resulting in a generally higher $B_{\text{tot}} = \sum_{i,j} |\mathbf{B}|_{i,j}$, the speed at which the instability grows due to the counterpropagating currents is largely unaffected by it.

The filamentation of the plasma leads to an interesting characteristic in the energy spectrum of the leptons: Whereas the bulk of the particles follow a thermal-like distribution with a maximum at low energies, a distinct peak emerges at the tail of the spectrum (see Fig. 5).

The high-energy electrons that make up this peak are homogeneously distributed in the "positron areas" (cf. Fig. 6). In this area the *z* component of the electric field that normally counteracts the movement of the leptons, will be accelerating instead of decelerating for particles of the opposite charge, leading to the prominent peak.

Similarly, the positron energy spectrum exhibits a peak (not shown here). These particles are again located within a filament of the opposite species, i.e., in an electron filament. The energy spectrum of the hadrons is largely thermal, with a kink at low energies that is due to the force accelerating the whole system (cf. Fig. 5).

While the overall behavior of the plasma can be well understood, some individual particle trajectories are quite complicated, as they interact with the strong fields of the border regions between filaments (see Fig. 7).

Such trajectories include reflection during their motion along the edge, similar to the motion in a magnetic bottle. The trajectory of a lepton moving near a border field will get bent along that border, making crossing that border difficult.

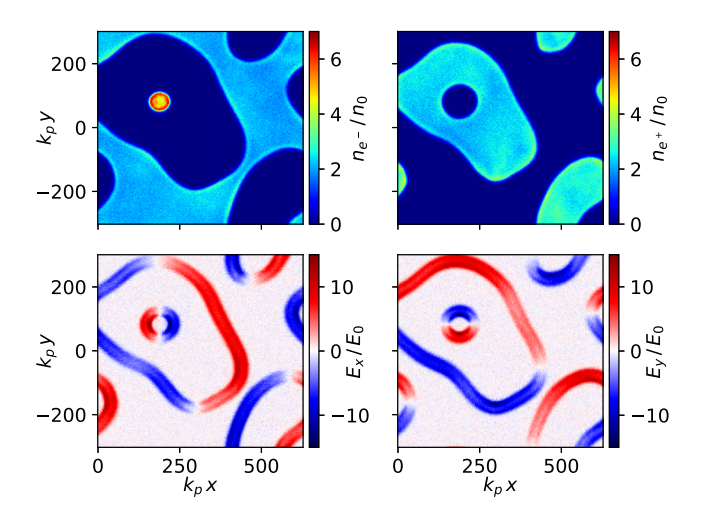


FIG. 2. Electron (upper left) and positron (upper right) densities, showing a distinct spatial inversion and the in-plane electric field components (lower) at time $\omega_p t \approx 3000$. Fields are normalized to $B_0 = E_0 = m_e c \omega_p / e$.

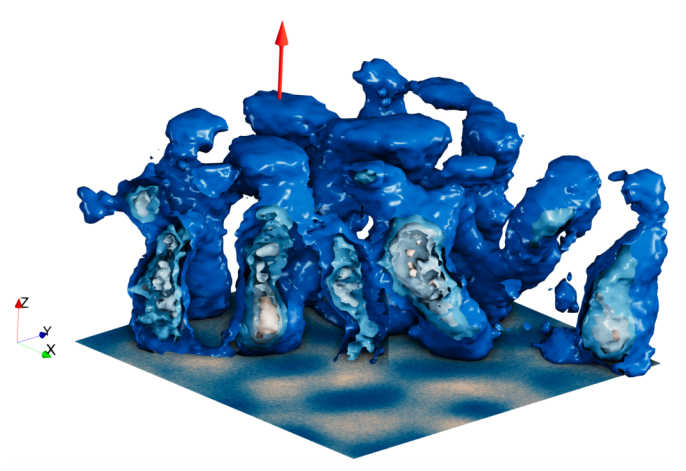


FIG. 3. Isosurfaces of electron density for a three-dimensional simulation with $p_{\parallel}=100m_ec$, $p_{\perp}=1m_ec$ at time $\omega_pt\sim 3000$. The bottom plane shows a 2D cut of the density in the *x-y* plane. The red arrow denotes the direction of the external forces.

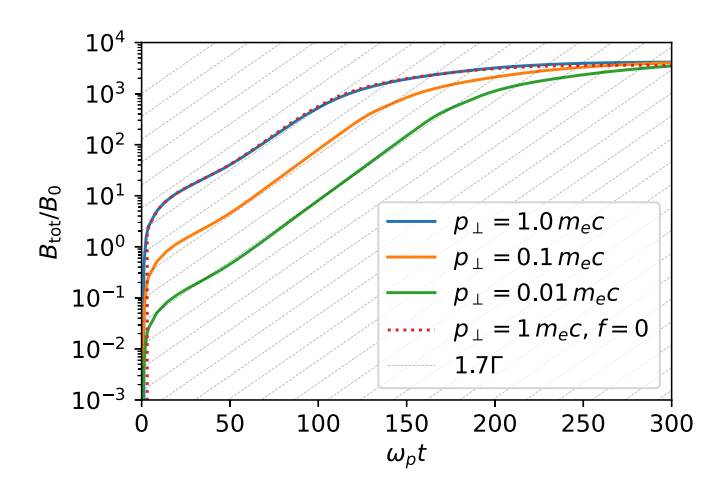


FIG. 4. Time evolution of the instability for multiple initial transversal momenta in two dimensions. The gray lines indicate the growth rate in terms of Eq. (12). The red dotted line indicates the case without external force.

As such we expect the borders to be largely void of leptons and therefore make annihilation along the borders unlikely. Furthermore, the leptons near the border are the most energetic, dampening the annihilation along the border even further, as $\sigma_{\rm ann} \sim \log \varepsilon/\varepsilon$. The exact behavior of matter and antimatter near the border and its consequences for the annihilation rate and subsequent radiation profile is quite involved and may be studied more in depth in a separate publication.

We considered a force that is small, $f \ll e^2 \sqrt{n/\pi r_0}$, such that the underlying separation mechanics do not change. However, for larger forces, namely when the force is larger than the stopping force, the separation mechanic breaks down as seen in Fig. 8. Forces of moderate strength can lead to stronger border fields and wider particle-free zones.

IV. ANALYTICAL MODEL

At the early stage, where $\delta n \ll n_0$, we can treat the instability as a small perturbation of a system in equilibrium.

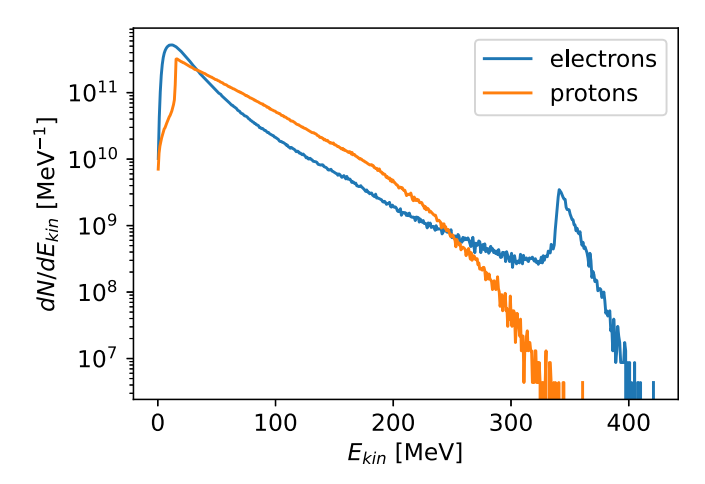


FIG. 5. Energy spectrum of electrons and protons at time $\omega_p t \approx$ 2500.

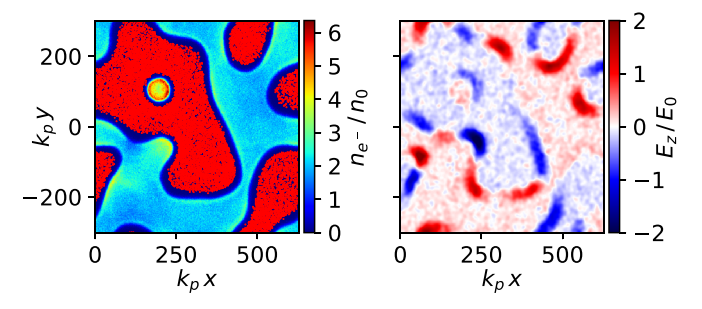


FIG. 6. The electron density (left) and the spatial positions of the energy-peak electrons ($E_{e^-} > 300$ MeV) at time $\omega_p t \approx 2500$. Each red dot corresponds to a numerical particle. On the right is the longitudinal electric field after a Gaussian filter has been applied.

Accordingly, we can describe the dynamics of the system using multifluid magnetohydrodynamics.

For simplicity, we assume an equal initial density for all particle species $n_0 = n_{0e^-} = n_{0e^+} = n_{0p^+} = n_{0p^-}$. Furthermore, we assume that leptons that flow along the z axis initially with the same momentum $\mathbf{p}_{0e^-} = \mathbf{p}_{0e^+} = p_0 \mathbf{e}_z$ and $|\mathbf{p}_0| \gg mc$, i.e., the particles are ultrarelativistic. This configuration is charge and current neutral and therefore in equilibrium. However, as the streams of electrons and positrons correspond to currents of opposite directions, this configuration is unstable. The opposite currents repel each other and start to separate in space transversely to their direction. This separation of leptons pulls hadrons of opposite charge as the charge neutrality must be satisfied. As the electrons and protons must have the same density, we denote it as $n_m = n_{e^-} = n_{p^+}$. Similarly, we denote the antimatter particles as $n_a = n_{e^+} = n_{p^-}$. For simplicity's sake we omit the constant force f_{CS} here.

The continuity equations are

$$\partial_t n_i + \nabla \cdot (n_i \mathbf{v}_i) = 0, \tag{7}$$

where the index i denotes either sort of particles. The equations of motion for the leptons

$$\gamma m[\partial_t \mathbf{v}_i + (\mathbf{v}_i \cdot \nabla) \mathbf{v}_i] = e_i \mathbf{E} - \nabla P / n_0 + \frac{e_i}{c} \mathbf{v}_i \times \mathbf{B}.$$
 (8)

Here, $i = \{e^-, e^+\}$, $\gamma = \text{const}$ is the relativistic γ factor of the leptons, m is their mass, and P = nT the thermal pressure term. The equations of motion for hadrons is

$$M\partial_t \mathbf{v}_i = e_i \mathbf{E}$$
, (9)

with $i = \{p^-, p^+\}$ and M is the proton mass. The Alfvén law is

$$\nabla \times \mathbf{B} = \frac{4\pi}{c} \mathbf{j}.\tag{10}$$

Here, we omit the contribution from the displacement current, which is valid for $k \ll \omega_p/c$. We make the ansatz

$$n = n_0 + \delta n = n_0 + \delta n_0 \exp(\Gamma t - ikx). \tag{11}$$

Similarly, we assume the fields and momentum to have an identical, exponentially growing perturbation. Furthermore, we choose the instability wave vector to be in the x direction $\mathbf{k} = k\mathbf{e}_x$. The magnetic field has the only component $\mathbf{B} = B\mathbf{e}_y$ and the electric field $\mathbf{E} = E\mathbf{e}_x$.

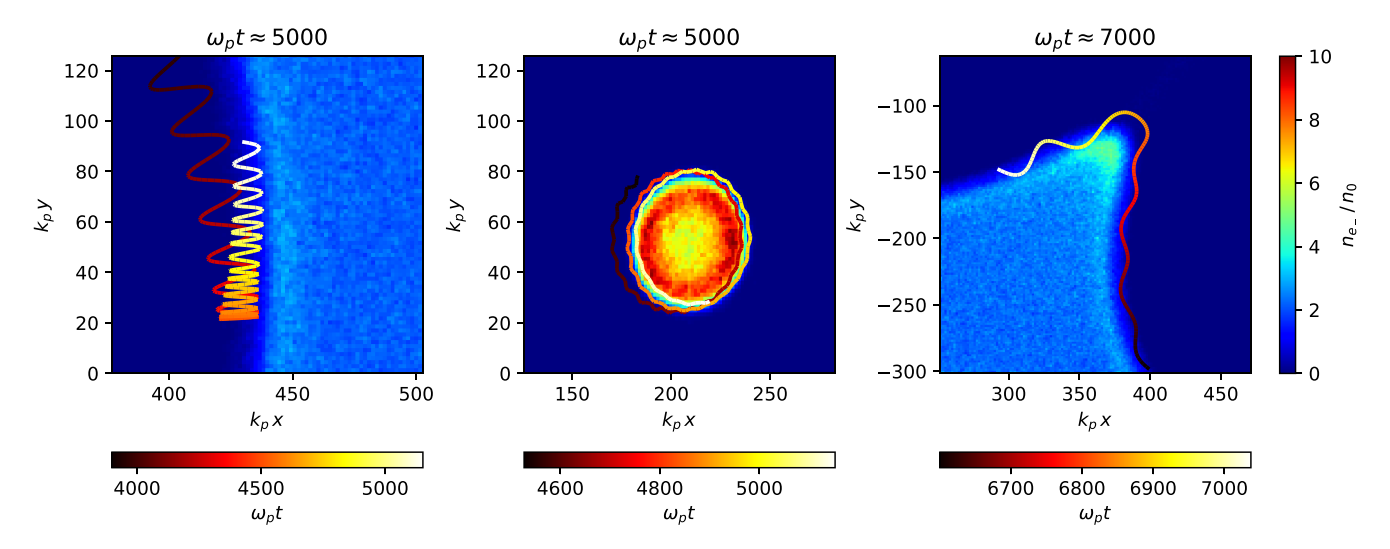


FIG. 7. Trajectories of singular electrons along filament edges, showing reflection (left), gyration (middle), and bending along filament edges (right).

From this we can calculate the dispersion relation for the instability

$$\Gamma = \sqrt{\omega_m^2 - k^2 c_s^2} = \sqrt{\frac{8\pi e^2 n_0}{M + \gamma m} - k^2 \frac{T}{M + \gamma m}},$$
 (12)

where ω_m is the combined "matter" plasma frequency defined by the total mass of the particles and $c_s = \sqrt{T/(M + \gamma m)}$ the sound velocity.

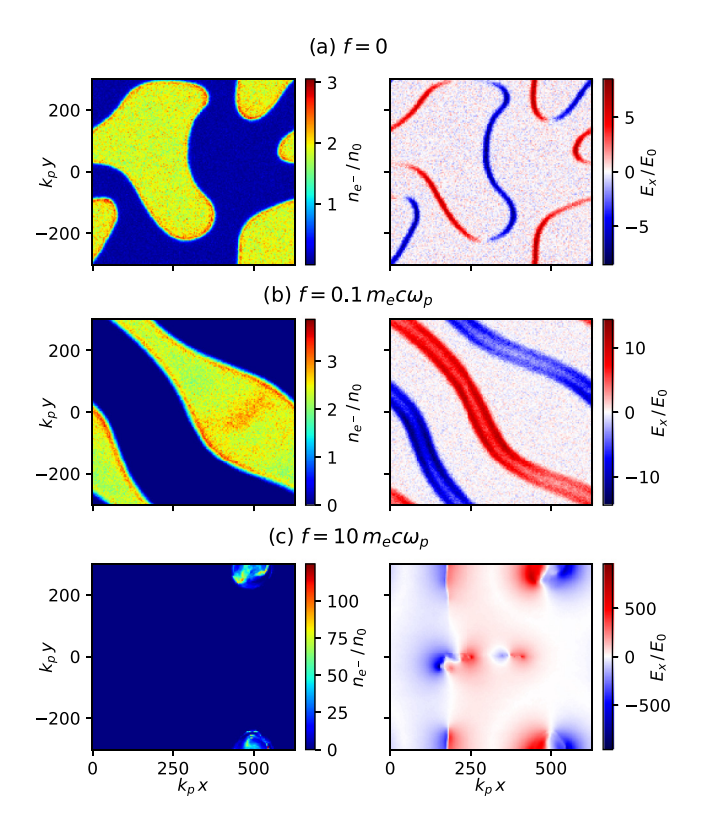


FIG. 8. Electron density (left) and E_x field (right) after $\omega_p t \sim$ 6000, for (a) no force, (b) a small force, and (c) a large force.

The predicted growth rate is in good agreement with the early stages of our simulation ($\omega_p t \leq 30$), as is shown in Fig. 4. At later stages, it deviates by a factor ~ 1.7 , indicating a breakdown of our linearization approximation. Additional simulations (not shown here) show that high-frequency perturbations may lead to the additional factor.

V. CONCLUSION

Using particle-in-cell simulations, we have demonstrated that a system consisting of homogeneously distributed electrons, positrons, protons, and antiprotons can separate into regions of matter and antimatter when exposed to a flux of photons. The force from the photon wind will accelerate the leptons creating counterpropagating currents, that while averaging out, result in a highly unstable equilibrium. Small density perturbations in this configuration grow exponentially, leading to the filamentation of the matter-antimatter plasma. The resulting structure consists of distinct regions of matter and antimatter, separated by bands of intense electromagnetic fields. The two- and three-dimensional simulation results are in strong agreement.

We observed the emergence of a distinct peak in the energy spectra of both electrons and positrons, originating from leptons confined in the filaments of the opposite species. These leptons are further accelerated by the stopping fields within the filaments.

Additionally, we studied the complex interactions of individual particles with the fields in the boundary regions between filaments. These interactions include processes such as reflection, gyration, and trajectory bending. Due to the strong separating border fields as well as the highly energetic leptons being near the border, this results in suppression of matter-antimatter annihilation.

Finally, we compared the simulation results with an analytical model derived from the linearization of magnetohydrodynamics, showing good agreement in describing the early stages of instability growth.

ACKNOWLEDGMENTS

This work has been supported by the Deutsche Forschungsgemeinschaft and by BMBF (Project 05P24PF1). We gratefully acknowledge the Gauss Centre for Supercomputing e.V. [33] for funding this project (lpqed) by providing computing time through the John von Neumann Institute for Computing (NIC) on the GCS Supercomputer JUWELS at Jülich Supercomputing Centre (JSC).

DATA AVAILABILITY

The data that support the findings of this article are not publicly available upon publication because it is not technically feasible and/or the cost of preparing, depositing, and hosting the data would be prohibitive within the terms of this research project. The data are available from the authors upon reasonable request.

- [1] G. Steigman, Observational tests of antimatter cosmologies, Annu. Rev. Astron. Astrophys. 14, 339 (1976).
- [2] G. Steigman, When clusters collide: constraints on antimatter on the largest scales, J. Cosmol. Astropart. Phys. 2008, 001 (2008).
- [3] J. Alcaraz, D. Alvisi, B. Alpat, G. Ambrosi, H. Anderhub, L. Ao, A. Arefiev, P. Azzarello, E. Babucci, L. Baldini, M. Basile, D. Barancourt, F. Barao, G. Barbier, G. Barreira, R. Battiston, R. Becker, U. Becker, L. Bellagamba, P. Béné, J. Berdugo, P. Berges *et al.*, Search for antihelium in cosmic rays, Phys. Lett. B 461, 387 (1999).
- [4] L. Canetti, M. Drewes, and M. Shaposhnikov, Matter and antimatter in the universe, New J. Phys. 14, 095012 (2012).
- [5] M. Giovannini, Probing large-scale magnetism with the cosmic microwave background, Class. Quantum Grav. 35, 084003 (2018).
- [6] M. Giovannini, The magnetized universe, Int. J. Mod. Phys. D 13, 391 (2004).
- [7] P. P. Kronberg, Extragalactic magnetic fields, Rep. Prog. Phys. 57, 325 (1994).
- [8] J. Rafelski, J. Birrell, A. Steinmetz, and C. T. Yang, A short survey of matter-antimatter evolution in the primordial universe, Universe 9, 309 (2023).
- [9] C. Grayson, C. T. Yang, M. Formanek, and J. Rafelski, Electron-positron plasma in BBN: Damped-dynamic screening, Ann. Phys. 458, 169453 (2023).
- [10] R. Blandford and R. Znajek, Electromagnetic extraction of energy from kerr black holes, Mon. Not. R. Astron. Soc. 179, 433 (1977)
- [11] M. C. Begelman, R. D. Blandford, and M. J. Rees, Theory of extragalactic radio sources, Rev. Mod. Phys. **56**, 255 (1984).
- [12] T. Piran, Towards understanding gamma-ray bursts, arXiv:astro-ph/9507114.
- [13] M. Lobet, X. Davoine, E. d'Humières, and L. Gremillet, Generation of high-energy electron-positron pairs in the collision of a laser-accelerated electron beam with a multipetawatt laser, Phys. Rev. Accel. Beams 20, 043401 (2017).
- [14] C. Huntington, F. Fiuza, J. Ross, A. Zylstra, R. P. Drake, D. Froula, G. Gregori, N. Kugland, C. Kuranz, M. Levy *et al.*, Observation of magnetic field generation via the Weibel instability in interpenetrating plasma flows, Nat. Phys. 11, 173 (2015).
- [15] G. Sarri et al., Generation of neutral and high-density electronpositron pair plasmas in the laboratory, Nat. Commun. 6, 6747 (2015).
- [16] G. Sarri, W. Schumaker, A. Di Piazza, M. Vargas, B. Dromey, M. E. Dieckmann, V. Chvykov, A. Maksimchuk, V. Yanovsky, Z. H. He, B. X. Hou, J. A. Nees, A. G. R. Thomas, C. H. Keitel, M. Zepf, and K. Krushelnick, Table-top laser-based source of

- femtosecond, collimated, ultrarelativistic positron beams, Phys. Rev. Lett. **110**, 255002 (2013).
- [17] G. Fiksel, W. Fox, A. Bhattacharjee, D. H. Barnak, P.-Y. Chang, K. Germaschewski, S. X. Hu, and P. M. Nilson, Magnetic reconnection between colliding magnetized laser-produced plasma plumes, Phys. Rev. Lett. 113, 105003 (2014).
- [18] A. Samsonov and A. Pukhov, Production and magnetic self-confinement of e^-e^+ plasma by an extremely intense laser pulse incident on a structured solid target, arXiv:2409.09131 [physics.plasm-ph].
- [19] E. F. van Dishoeck, Laboratory astrophysics: Key to understanding the universe, Proc. Int. Astron. Union 15, 3 (2019).
- [20] G. K. Ngirmang, J. T. Morrison, K. M. George, J. R. Smith, K. D. Frische, C. Orban, E. A. Chowdhury, and W. M. Roquemore, Evidence of radial weibel instability in relativistic intensity laser-plasma interactions inside a sub-micron thick liquid target, Sci. Rep. 10, 9872 (2020).
- [21] C. D. Arrowsmith, P. Simon, P. J. Bilbao, A. F. A. Bott, S. Burger, H. Chen, F. D. Cruz, T. Davenne, I. Efthymiopoulos, D. H. Froula, A. Goillot, J. T. Gudmundsson, D. Haberberger, J. W. D. Halliday, T. Hodge, B. T. Huffman, S. Iaquinta, F. Miniati, B. Reville, S. Sarkar, A. A. Schekochihin, L. O. Silva, R. Simpson, V. Stergiou, R. M. G. M. Trines, T. Vieu, N. Charitonidis, R. Bingham, and G. Gregori, Laboratory realization of relativistic pair-plasma beams, Nat. Commun. 15, 5029 (2024).
- [22] A. Kendl, G. Danler, M. Wiesenberger, and M. Held, Interchange instability and transport in matter-antimatter plasmas, Phys. Rev. Lett. **118**, 235001 (2017).
- [23] W. Greiner and J. Reinhardt, *Quantum Electrodynamics* (Springer, Berlin, 2003).
- [24] J. Carbonell, K. Protasov, and A. Zenoni, pp low energy parameters from annihilation cross section data, Phys. Lett. B **397**, 345 (1997).
- [25] A. Zenoni, A. Bianconi, F. Bocci, G. Bonomi, M. Corradini, A. Donzella, E. Lodi Rizzini, L. Venturelli, A. Bertin, M. Bruschi, M. Capponi, S. De Castro, R. Donà, D. Galli, B. Giacobbe, U. Marconi, I. Massa, M. Piccinini, N. Semprini Cesari, R. Spighi et al., New measurements of the p̄p annihilation cross section at very low energy, Phys. Lett. B 461, 405 (1999).
- [26] A. Bianconi, M. Corradini, M. Hori, M. Leali, E. Lodi Rizzini, V. Mascagna, A. Mozzanica, M. Prest, E. Vallazza, L. Venturelli, and N. Zurlo, Measurement of the antiproton– nucleus annihilation cross section at 5.3 MeV, Phys. Lett. B 704, 461 (2011).
- [27] T.-G. Lee and C.-Y. Wong, Nuclear annihilation by antinucleons, Phys. Rev. C **93**, 014616 (2016).

- [28] J. Carbonell and K. Protasov, Annihilation of ultra low energy antiprotons, Hyperfine Interact. **76**, 325 (1993).
- [29] A. Pukhov, Three-dimensional electromagnetic relativistic particle-in-cell code VLPL (virtual laser plasma lab), J. Plasma Phys. **61**, 425 (1999).
- [30] A. Pukhov, Particle-in-cell codes for plasma-based particle acceleration, in *Proceedings of the 2014 CAS-CERN Accelerator School: Plasma Wake Acceleration* (2016), Vol. 1.
- [31] K. Yee, Numerical solution of initial boundary value problems involving maxwell's equations in isotropic media, IEEE Trans. Antennas Propag. 14, 302 (1966).
- [32] E. S. Weibel, Spontaneously growing transverse waves in a plasma due to an anisotropic velocity distribution, Phys. Rev. Lett. 2, 83 (1959).
- [33] https://www.gauss-centre.eu/.